Lattice-gas model of methane and carbon dioxide sI clathrate hydrates: A comprehensive study using analytical cluster approximation and Monte Carlo simulations

P. Longone [1,*], F. O. Sanchez-Varretti [2], F. Bulnes [1], and A. J. Ramirez-Pastor [1]

[1] *Departamento de Física, Instituto de Física Aplicada (INFAP), Universidad Nacional de San Luis - CONICET, Ejército de Los Andes 950, D5700HHW, San Luis, Argentina*

[2] *Universidad Tecnológica Nacional, Facultad Regional San Rafael, Instituto de Física Aplicada (INFAP), CONICET, Gral. Urquiza 314, 5600, San Rafael, Mendoza, Argentina*

(Received 4 March 2024; revised 12 June 2024; accepted 12 November 2024; published 3 December 2024)

The thermodynamic properties of sI clathrate hydrates involving methane and carbon dioxide guest molecules have been investigated using Monte Carlo (MC) simulations in the grand canonical ensemble, and analytical cluster approximation (CA) theory. The CA approach is founded on the precise calculation of states within finite cells. Both the sI hydrate structure and the guest species were represented using a two-dimensional triangular lattice-gas model with single- and multiple-site occupancy. The investigation entailed monitoring the lattice coverage's dependence on the chemical potential (adsorption isotherm) and examining quantities like Helmholtz free energy, energy of the adsorbed phase, configurational entropy, and adsorption heat. Three distinct scenarios were considered, each dependent on the intra- and interspecies interactions. First, the study was restricted to an ideal clathrate hydrate, wherein lateral interactions were disregarded, and the system's properties are governed by entropy alone. Second, lateral interactions between the guest species and water molecules were introduced by employing the well-established Lorentz-Berthelot mixing rules. Lastly, repulsive lateral interactions were taken into account. In all cases, a remarkable agreement between the results obtained through CA and MC was observed, underscoring the significant potential of CA theory as a valuable tool for exploring cavity occupancy and selectivity in the sI clathrate hydrate formation process.

DOI: 10.1103/PhysRevE.110.064103

I. INTRODUCTION

Clathrate hydrates are nonstoichiometric compounds in which a gas with low solubility is trapped in a crystalline lattice of cavities made up of water molecules [1,2]. The water molecules tend to organize themselves in such a way that the presence of a gas molecules (guest species) does not substantially alter the nature of hydrogen bonds. The partial adsorption of the guest molecules within their cavities gives stability to the system, hence forming clathrate hydrates of gases. The conditions that promote the formation of hydrates include low temperatures and high pressures in natural and artificial environments. Different crystalline structures can be formed, depending on the size and properties of guest molecules and, up to now, three different clathrate hydrate structures are known: two cubic structures known as structures I (sI) and II (sII) [3–5], and a hexagonal structure known as structure H (sH) [6,7]. In particular, natural guest species such as methane (CH_4) and carbon dioxide (CO_2) result into the formation of structure sI. Inside of these structures, each unit cell contains two dodecahedron cavities (5^{12}) (small cavity) and six tetrakaidecahedron cavities ($5^{12}6^2$) (large cavity). The symbols between parentheses correspond to Jeffrey's notation of cavities [8,9]. It may be noted that the sI structure is essentially the same as that put forward by Weaire and Phelan [10] to solve the Kelvin problem [11], which was concerned with finding a foam that would possess a minimal surface area between bubbles. This result indicates that the structure that a clathrate hydrate takes is related to the geometry of the gas molecule, and so the fundamental intermolecular interactions governing clathrate hydrate behavior are not related to the structure per se but the species involved [12].

Clathrate hydrates of CH_4 and CO_2 occur quite frequently in the form of deposits in the deep oceans and in Arctic permafrost regions [13–15], being considered of significant industrial importance. In this respect, there is a major interest in the determination of the formation conditions of clathrate hydrates for a variety of reasons. These hydrates can constitute a valuable resource because they appear in natural gas fields [16]. It has been estimated that the total amount of energy available from the natural gases trapped in these hydrates exceeds that available from all the conventional fossil fuels combined [2]. It is also believed that the decomposition of natural gas clathrate hydrates may have influenced past climate changes [17]. In addition, clathrate hydrates are essential and needed for many industrial activities and processes, such as carbon dioxide sequestration [18], water desalination [19], or storage of energy-carrier methane gases [20,21].

From a theoretical point of view, phase equilibria in clathrate hydrate systems is frequently described using the statistical mechanical van der Waals-Platteeuw theory [22]. The main assumptions of this theory are (1) the interactions between the guest molecules and the aqueous lattice are

*Contact author: plongone@unsl.edu.ar

relatively weak and they are limited to the nearest neighbors (*nn*) of the gas molecule; (2) the interactions between host molecules corresponding to different cavities are neglected; and (3) multiple occupancy of the cavities by several gas guest molecules is not considered. Accordingly, the behavior of each guest molecule does not depend on the presence of other guest molecules. Later, some modifications were introduced to this model, such as multiple occupancy and flexibility of cavities [23–26]. In its original form, or with some modifications, the van der Waals-Platteeuw theory is currently the most important and widely used theoretical tool in the study of clathrate hydrates.

Despite the theoretical efforts devoted to understand the thermodynamics of clathrate hydrates, an exact statistical mechanical treatment of this problem is unfortunately not yet available, and, therefore, the use of computer simulations appears as a relevant way to study these systems. Several papers have been done in this line. Among them, Pimpalgaonkar *et al.* [27] determined, by using Monte Carlo (MC) simulations, the triple-point lines for methane and ethane hydrates. Papadimitriou *et al.* [28] reported the number of occupied cavities for He and THF mixed hydrates. The study showed that large cavities were completely occupied by THF molecules, whereas the small cavities were partially occupied by He atoms. The stability of the cavities that form the clathrate hydrates and the effects of lattice distortion when the cavities are occupied by guest species of different sizes have also been investigated by numerical simulations [29–32].

In recent papers from our group, a two-dimensional (2D) lattice-gas model with multiple site occupancy, supplemented by MC simulations was developed for the study of the stability and distortion of sI structure in methane, carbon dioxide, and ethylene clathrate hydrates [33–35]. Based on calculations of the degree of deformation of the lattice and the free energy per site of the adsorbed phase, (i) the stability of the sI structure was investigated, and (ii) the pressure-temperature phase diagrams were obtained and compared with theoretical as well as experimental predictions from the literature. In particular, Ref. [35] is devoted to study of the CO_2-CH_4 exchange process in sI clathrate hydrates. This paper argues that the CO_2-CH_4 exchange process is driven by the entropy of the different species rather than by the lateral interactions between them. In addition, Refs. [33–35] showed that (i) the 2D lattice-gas model captures the essence of the phenomena of distortion and stability in clathrate hydrates with a reduced number of parameters, and (ii) the use of a 2D approach facilitates the calculations and the analysis of the results.

On the other hand, in recent years, our research group has made several contributions to the study of monolayer adsorption considering both single- and multiple-site occupancy [36–40]. In Refs. [36–40], we employed a cluster approximation (CA), which is based on the precise calculation of configurations within finite cells. This theoretical approach has been successfully applied to investigate the behavior of adsorbed monolayers in the presence of additive and nonadditive lateral interactions.

The utilization of CA models to describe hydrate clathrate frameworks presents a promising avenue for the development of simplified and solvable models. These strategies have the potential to significantly enhance our comprehension of the thermodynamics associated with clathrate hydrates in a two-dimensional setting [33–35]. In this context, the main objectives of this work are (i) to develop a generalization of the classical CA [41–43] to study the problem of non-flexible sI clathrate hydrates (not considering lattice distortion effects). CA is a brute force approximation to the system's partition function, which allows to obtain the main thermodynamic quantities, such as total coverage (or coverage of cavities), system energy, entropy per site, free energy and heat of adsorption, etc.; (ii) to evaluate the scope and limitations of CA through the exhaustive comparison between theoretical data and MC simulation results; and (iii) to apply the combined MC plus CA scheme to obtain new results, particularly concerning the incorporation of repulsive interactions between guest molecules. Objectives (i) and (ii) are of methodological interest (see Secs. III A and III B), while objective (iii) aims to enhance the understanding of repulsive lateral interactions as an effective way to introduce steric hindrance in the system (see Sec. III C).

The present study is a natural continuation of our previous work and complements the results obtained in Refs. [33–35]. Here, we introduce new developments based on exact calculation of adsorption states in small systems. On the basis of this simple theoretical model, we hope to contribute to a better understanding of a system governed by a large number of parameters and whose theoretical and experimental treatment is rather difficult.

The paper is organized as follows: the model and basic definitions are introduced in Sec. II, the results are presented and discussed in Sec. III. and, finally, Sec. IV is devoted to conclusions.

II. MODEL AND BASIC DEFINITIONS

Following the arguments given in Refs. [33,34], the structure of sI gas hydrates in the presence of guest species is modeled in the framework of a 2D lattice-gas approximation. A 2D triangular lattice is used to represent the substrate, as shown in Fig. 1(a). Some lattice sites are occupied by water molecules, the *W* sites, which form hexagonal structures on the substrate with an empty site in the center of each hexagon, labeled as *C* sites; in addition a particular set of sites, identified as *O* sites, appear at the same plane as the hexagons formed by the water molecules. The *S* sites in Fig. 1(a) are the available ones for guest molecules under favorable conditions. The *S* sites form domains or cavities, namely small cavities and large cavities. The scheme is completed with the guest molecules.

In the present paper two different guest molecules have been considered, methane (CH_4) and carbon dioxide (CO_2). According to the model, it is assumed that methane molecules, with tetrahedral geometry [44], can be adsorbed in such a way that three vertices (*H*) of the molecule occupy three *nn S* sites on the lattice [see Fig. 1(b)]. On the other hand, carbon dioxide molecules, with linear geometry [44], can be adsorbed occupying a linear chain of three consecutive *S* lattice sites [see Fig. 1(c)]. Additionally, it is assumed that (1) guest molecules are absorbed or desorbed without any

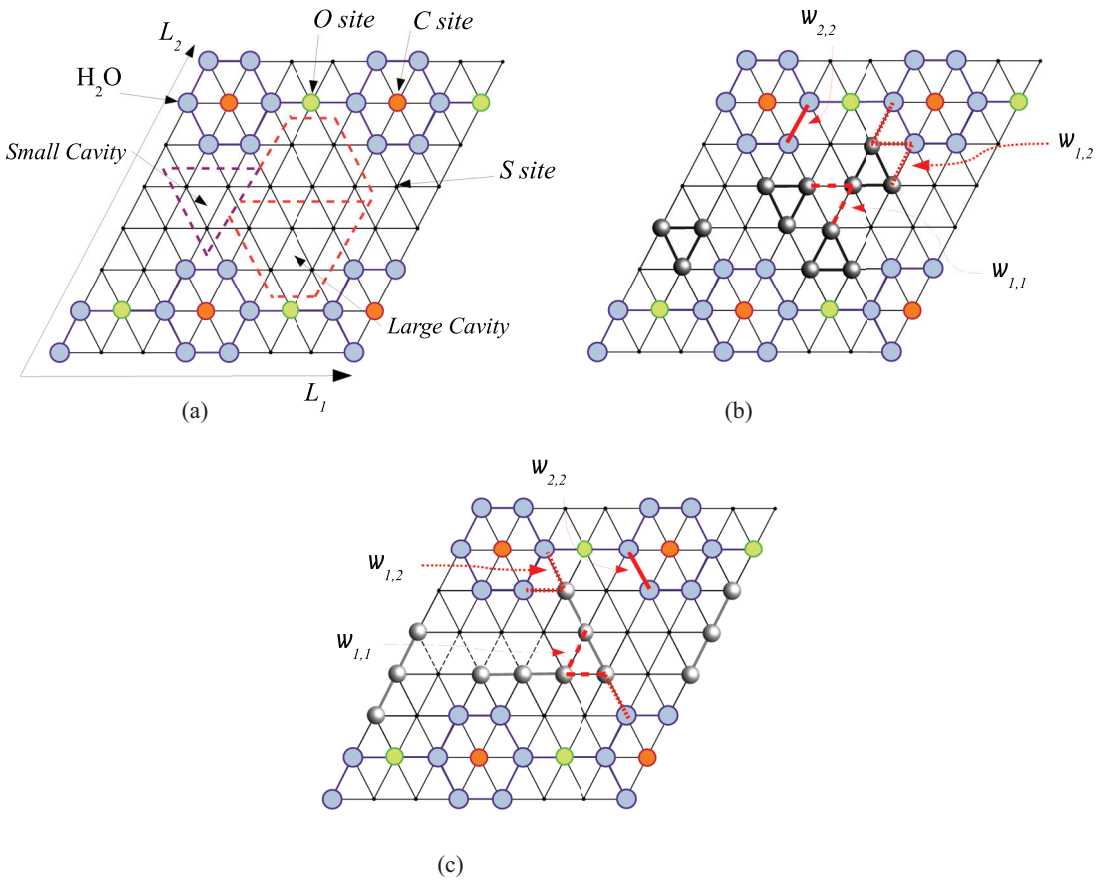

FIG. 1. (a) 2D lattice gas model for the sI structure of clathrate hydrates. Guest molecules could adsorb on S sites, which are arranged in domains identified as small and large cavities. The W and O sites are occupied by water and oxygen molecules respectively, while the C sites are also unavailable for guest molecules. (b) Schematic representation showing the adsorption of guest methane species. (c) The same as panel (a) for carbon dioxide host species.

possible dissociation; and (2) based on previous studies in the literature [29,31,45,46], guest molecules are considered rigid. Therefore, their vibrational degrees of freedom are not included in the calculations.

The cost of introducing the lattice-gas model described in this section is the lack of some experimental features presented by real clathrates, mainly the loss of a degree of freedom. However, even with the simplification of the problem to a 2D discrete lattice, the model proposed here retains the symmetry of the sI hydrate structure and the relative sizes of the guest molecules. As showed in previous work [33–35], these properties seem to capture the essence of the real systems. Interested readers are referred to Refs. [33–35] for a more complete description of the mapping between the real system and the 2D model used here.

Let us consider a lattice of size $M_0 = L_1 \times L_2$ sites. Then, the number of available adsorption sites for the guest molecules (S sites) is $M = M_0 - (n_W + n_O + n_C)$, where n_W, n_O, and n_C are, respectively, the number of W, O, and C sites. In order to describe the system consisting of N adsorbed molecules on M sites at a given temperature T, the occupation variable c_i is introduced. This variable can take different values according to $c_i = 0$ if site i is empty, $c_i = 1$ if site i is occupied by a guest molecule, $c_i = 2$ for a W site, and $c_i = 3$ for an O site. Under such conditions, the system is characterized by the Hamiltonian

$$H = \sum_{\langle i,j \rangle} \left[w_{11}\delta_{c_i,1}\delta_{c_j,1} + w_{22}\delta_{c_i,2}\delta_{c_j,2} + w_{12}\left(\delta_{c_i,1}\delta_{c_j,2} + \delta_{c_i,2}\delta_{c_j,1}\right)\right] - kNw_{11}, \quad (1)$$

where $\langle i, j \rangle$ means that the sum runs over pairs of nn lattice sites and w_{mn} is a lateral energy interaction associated with the occupancy of both sites i and j. The labels m and n ($m, n = 1, 2, 3$) are used to identify the molecules involved in the interaction according to 1 for a guest molecule, 2 for a W site, and 3 for an O site. For instance, w_{11} is the energy interaction for a pair of nn sites occupied by guest molecules. See Fig. 1. As in Refs. [33,34], the interactions w_{13} and w_{23} are considered to be zero in the present work. The last term in the Hamiltonian, $-kNw_{11}$, is introduced because the summation over all the pairs of nn sites would overestimate the total energy by adding kN internal bonds belonging to the N adsorbed guest molecules. In this case [see Figs. 1(b) and 1(c)], $k = 3$ and $k = 2$ correspond to CH_4 and CO_2 molecules, respectively.

Finally, w_{11}, w_{12}, and w_{22} have been obtained by using the standard Lorentz-Berthelot mixing rules [47–50]. In this framework, guest-guest, water-guest, and water-water lateral

interactions can be written as

$$w_{mn} = \frac{l_{mn}\sqrt{\varepsilon_m \varepsilon_n}}{r}, \tag{2}$$

where l_{mn} is an interaction parameter that can be correlated to experimental cage occupancy data. As in Refs. [33,34], in this work it is assumed that $l_{mn} = 1$. ε_m (ε_n) represents the characteristic energy corresponding to the m (n) species. The values of ε_m (ε_n) were taken from Table 2 in Ref. [50]. Interested readers are referred to Ref. [51] for a more complete description of the calculations used to determine ε_m (ε_n). If $m = n$, Eq. (2) corresponds to intraspecies interactions. If $m \neq n$, Eq. (2) represents interspecies interactions. Given that w_{mn} represents the site-site lateral interaction, a factor r is used in the denominator of Eq. (2) because of the number of lattice sites that occupy the guest molecules, in this case $r = 3$ for both CO_2 and CH_4 molecules.

A. Monte Carlo simulation

The adsorption process is simulated through MC simulations in the grand canonical ensemble [52–54]. First of all a triangular lattice of size $M_0 = L_1 \times L_2$ sites is generated, with periodical boundary conditions, and the positions of W, O, C, and S sites are identified. Then, the MC simulation is carried out according to the following scheme:

(1) The values of chemical potential μ and temperature T are set.

(2) An elementary Monte Carlo step (MCS) is performed.

(2.1) A set of adjacent sites is chosen at random, according to the shape of the guest molecule. Then, a random number $\xi \in [0, 1]$ is generated.

(2.2) If the selected sites are empty, an attempt is made to adsorb a molecule. A guest molecule is adsorbed if $\xi < W_{\text{ad}}$.

(2.3) If the selected sites are found occupied by exactly one guest molecule, an attempt is made to desorb the molecule. Accordingly, the molecule is desorbed if $\xi < W_{\text{des}}$.

(2.4) Otherwise, any attempt is rejected.

(2.5) Repeat from step (2.1) M times.

(3) Repeat from step (2) m times.

W_{ad} (W_{des}) is the adsorption (desorption) probability for a guest molecule, according to the Metropolis scheme of probabilities. $W_{\text{ad}} = \min\{1, \exp[-\beta(\Delta H - \mu)]\}$, and $W_{\text{des}} = \min\{1, \exp[-\beta(\Delta H + \mu)]\}$, with $\Delta H = H_f - H_i$ being the difference between the Hamiltonians of the final and initial states [55]; $\beta = (k_B T)^{-1}$, and k_B is the Boltzmann constant.

In our case, the equilibrium state can be well reproduced after discarding the first $m_0 = 10^7$ MCS. Then, averages have been evaluated over $m_1 = 10^7$ successive configurations.

Thermodynamic quantities, such as surface coverage θ, coverage of cavities θ_{cavity}, and energy per site u, are obtained as simple averages,

$$\theta = \frac{r\langle N\rangle}{M}, \tag{3}$$

$$\theta_{\text{cavity}} = \frac{\langle N\rangle}{M_{\text{cav}}}, \tag{4}$$

and

$$u = \frac{\langle H\rangle}{M}, \tag{5}$$

where r is the number of lattice sites occupied by one guest molecule [see Eq. (2)], M_{cav} is the number of cavities in the lattice, and the thermal average $\langle \dots \rangle$ means the average throughout the m_1 MCSs.

In the case of differential heat of adsorption, q_d, more calculations are required [52,56],

$$q_d = \left[-\frac{\partial\langle H\rangle}{\partial\langle N\rangle}\right]_T = -\frac{\langle HN\rangle - \langle H\rangle\langle N\rangle}{\langle N^2\rangle - \langle N\rangle^2}, \tag{6}$$

where $\langle HN\rangle$, $\langle H\rangle$, $\langle N\rangle$, and $\langle N^2\rangle$ can be evaluated via MC simulations in the grand canonical ensemble.

The estimation of the quantities in Eqs. (3)–(6) is rather straightforward from averaging over a large enough number of instantaneous configurations (states) of a thermodynamic system. However, free energy and entropy are much more difficult to evaluate, and they cannot be directly computed [52,57]. To calculate free energy and entropy, various methods have been developed [58–61]. Among them, the thermodynamic integration method (TIM) is one of the most widely used and practically applicable [57–59,62].

In the grand canonical ensemble, the thermodynamic integration method relies upon integration of the chemical potential μ on coverage along a reversible path between an arbitrary reference state and the desired state of the system. This calculation also requires the knowledge of the total energy U for each obtained coverage. Thus, for a system made of N particles on M lattice sites, we have

$$\mu = \left(\frac{\partial F}{\partial N}\right)_{M,T}. \tag{7}$$

It follows that

$$F(M, N, T) = F_0(M, N_0, T) + \int_{N_0}^{N} \mu dN, \tag{8}$$

and

$$S(M, N, T) = S_0(M, N_0, T) + \frac{U(M, N, T) - U_0(M, N_0, T)}{T} - \frac{1}{T}\int_{N_0}^{N} \mu dN. \tag{9}$$

In our case, the determination of the entropy and the energy in the reference state, $S_0(M, N_0, T)$ and $U_0(M, N_0, T)$, respectively, is trivial [$S_0(M, N_0, T) = U_0(M, N_0, T) = 0$ for $N_0 = 0$]. Then, writing the last equation in terms of intensive variables, the free energy per site ($f = F/M$) and configurational entropy per site ($s = S/M$) give

$$\beta f(\theta, T) = \frac{1}{k_B T}\int_0^{\theta} \frac{\mu}{r} d\theta, \tag{10}$$

and

$$\frac{s(\theta, T)}{k_B} = \frac{u(\theta, T)}{k_B T} - \frac{1}{k_B T}\int_0^{\theta} \frac{\mu}{r} d\theta. \tag{11}$$

The curve of μ vs θ can be obtained from Eq. (3). In our MC simulations, the chemical potential μ is varied, then the coverage dependence $\theta(\mu)$ is obtained. In addition, $u(\theta, T)$ can be obtained from Eq. (5).

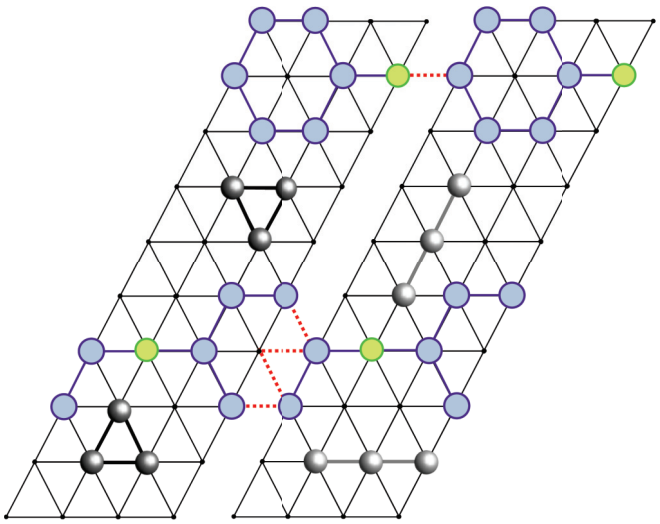

FIG. 2. On the left, a cluster of size $M_c = 4 \times 10 = 40$ sites. A small portion of the lattice represented in the previous figure. The cluster is replicated on the right to highlight the relevance of periodic boundary conditions.

B. Cluster approximation

In the framework of the cluster approximation, it is assumed that the behavior of the whole system can be approximately reproduced by the behavior of a small "portion" of the system. Accordingly, a small cell of lattice sites called the "cluster" is selected. The size and the shape of the cluster are chosen in such a manner that it could be used to generate the whole lattice by repetition, like a building block.

The importance of the cluster approximation relies on the fact that it is possible to evaluate the partition function of the cluster exactly, and therefore allows to determine analytically the main thermodynamic quantities for the system.

In order to apply the CA formalism to the present work, a triangular cluster of size $M_c = l_h \times l_w$ adsorption sites is considered, with periodic boundary conditions, where $M_c \ll M$, with M being the size of the system. As an example, Fig. 2 shows a cluster of size $M_c = 40$ sites.

The exact grand partition function for the cluster can be written as follows:

$$\Xi = \sum_k \Xi_k, \tag{12}$$

where k labels the different configurations of particles in the cluster, so that Ξ_k is the contribution of the configuration k to the grand partition function Ξ. Thus,

$$\Xi_k = g_k(E_k) \exp\left[\beta(\mu N_k - E_k)\right]. \tag{13}$$

For a given configuration k, N_k, and E_k are, respectively, the number of occupied S sites and the total nn energy interaction in the cluster. $g_k(E_k)$ is used for taking into account a possible degeneracy in energy E_k.

Then, in the framework of the cluster approximation, the adsorption isotherm for a cluster of size M_c sites can be evaluated as follows:

$$\theta(\mu) = \frac{1}{M_c}\langle N \rangle, \tag{14}$$

where

$$\langle N \rangle = \frac{1}{\Xi}\sum_k \Xi_k N_k \tag{15}$$

is the mean number of occupied cluster sites for chemical potential μ. The mean energy of the system is

$$\langle U \rangle = \frac{1}{\Xi}\sum_k \Xi_k E_k, \tag{16}$$

and the resulting mean energy per adsorption cluster site is $\langle u \rangle = M_c^{-1}\langle U \rangle$.

On the other hand, the differential heat of adsorption can be written as [63]

$$q_d(\mu) = -\frac{\langle UN \rangle - \langle U \rangle \langle N \rangle}{\langle N^2 \rangle - \langle N \rangle^2}, \tag{17}$$

where

$$\langle UN \rangle = \frac{1}{\Xi}\sum_k \Xi_k N_k E_k, \tag{18}$$

and

$$\langle N^2 \rangle = \frac{1}{\Xi}\sum_k \Xi_k N_k^2. \tag{19}$$

Finally, the configurational entropy of the adsorbed phase can be written as [64]

$$S(\theta, T) = k_B \frac{\partial}{\partial T}[T \ln \Xi], \tag{20}$$

$$s(\theta, T) = \frac{S(\theta, T)}{M} = \frac{1}{M}\left\{k_B \ln \Xi + \frac{1}{T}[\langle U \rangle - \mu M_c \theta]\right\}, \tag{21}$$

while the Helmholtz free energy F can be obtained from

$$F(\theta, T) = \langle U \rangle - TS, \tag{22}$$

$$f(\theta, T) = \frac{F(\theta, T)}{M} = \frac{1}{M}(-Tk_B \ln \Xi + \mu M_c \theta). \tag{23}$$

III. RESULTS AND DISCUSSION

In the present section, the adsorption isotherm (the coverage degree in terms of the number of cavities θ_{cavity} as a function of the chemical potential $\beta\mu$), adsorption energy, adsorption heat (or encapsulation heat), configurational entropy, and Helmholtz free energy of the adsorbed phase are obtained by CA and compared with MC simulation predictions. It is important to note that knowledge of the Helmholtz free energy allows us to derive all necessary thermodynamic quantities in a consistent way [64]. In addition, as shown in Ref. [34], the behavior of the Helmholtz free energy relates to the stability of sI structure (the minimum values of the free energy allow us to determine the stability region to the clathrate hydrate).

It is important to highlight several real features of clathrate hydrates that were not included in our model. (i) The coexistence of liquid water, ice-hydrate, and host molecules was not considered at the onset of the simulations. In both our work and other three-dimensional simulation studies [27–32], as well as in theoretical models [22], the solid hydrate phase is typically assumed to be an empty, stable structure—a

hypothetical phase without host molecules. (ii) Interactions between host molecules and water, or between the hosts themselves, were modeled as first-neighbor (NN) interactions, without taking into account the relative positions of the species or long-range interactions, such as Coulombic forces. As described in Sec. II, these interactions were parameterized using the Lorentz-Berthelot equation (2), with an average value assigned to each monomer within a molecule. (iii) Methane was not modeled with its full tetrahedral geometry but was simplified to a triangular base in a 2D context. Further details on the representation of host molecules in our model can be found in previous studies [33–35]. (iv) The sI structure was modeled using a 2D lattice-gas model. This reduction to two dimensions, while eliminating one degree of freedom, preserves key symmetries, leading to a significant reduction in computational costs without compromising the essential physical and structural phenomena. This aspect should be considered in future studies for more direct comparison with experimental data. (v) The potential influence of ionic concentrations on the behavior of the solid phase was not included. It is known that the concentrations of anions and cations can affect clathrate formation, acting as inhibitors or promoters depending on their levels [65–70]. Including ions in the model could offer a significant improvement, allowing for studies more aligned with real experimental conditions.

The model presented here can be considered an initial coarse-grained approach designed to improve our understanding of fundamental phenomena in clathrate thermodynamics that are still not well understood. One such example is the displacement of CH_4 by CO_2 in clathrates [45]. Despite the numerous studies on this subject, many lack sufficient experimental evidence to fully explain the underlying mechanism of CH_4 substitution by CO_2, leaving the phenomenon a topic of ongoing debate. Recently, using our model, we proposed a mechanism based on the competition of entropic forces between species [35], offering a simpler approach from the perspective of 2D lattice-gas models compared with continuous three-dimensional models.

The study is composed of three parts. In the first one (Sec. III A), lateral interactions are neglected ($w_{m,n}/k_BT = 0.0$). We called these systems "ideal clathrate hydrates." Under these conditions, species interact only through excluded volume interactions, and the adsorption-desorption process is governed by entropy alone. The second part (Sec. III B) deals with interacting adsorbates. Thus, real guest-guest and guest-water interactions are considered $w_{m,n}/k_BT < 0.0$. We refer to these systems as "real clathrate hydrates." The values of the lateral couplings are calculated by using the Lorentz-Berthelot mixing rules [see Eq. (2)] [47–50]. In Secs. III A and III B, comparative CA and MC studies are conducted to contrast the theoretical predictions with numeric simulations. Subsequently, taking advantage of these comparisons, the occupancy behaviors of cavities as well as the stability of hydrate clathrates in 2D are analyzed. Finally, in Sec. III C, repulsive lateral interactions are introduced $w_{m,n}/k_BT > 0.0$. Repulsive lateral interactions could play an important role because they represent the behavior of first-neighbor molecules with short-range interactions. Repulsive couplings between water and guest gas molecules prevent the collapse of the cavities that form the clathrate hydrate structure, contributing to the stability of the structure [1]. In this context, it is evident that repulsive interactions represent an equivalent to what is known as steric hindrance. This behavior can provide information to determine the degree and state of occupancy of both small and large cavities within the structure of the hydrate clathrate.

The MC simulations have been carried out using the 2D lattice-gas model and the scheme described in previous section. The lattice size used is $L_1 \times L_2 = 80 \times 128$ (3072 H_2O molecules and 512 O sites), which accurately represents the sI structure (finite-size effects are expected to be small). On the other hand, CA calculations have been performed for cells of size $m = 4 \times 10$ (see Fig. 2). In the case of CA, a C++ code made by the authors has been used to count all possible ways to arrange N guest molecules on M_c sites, with $0 \leqslant N \leqslant M_c/r$. Given the values of the input variables (system size M_c and lateral interaction energies), a finite number of nested cycles goes through all the adsorption states, thus allowing us to obtain the configurational factor $g(N, M_c)$, the grand canonical partition function, the adsorption isotherm, and the configurational entropy per site. As is usual in the case of clathrate hydrates, to achieve a better understanding of the behavior of the system, both the results of the MC simulations and those of the CA approximations are represented in terms of cavity coverage θ_{cavity}. The relationship between cavity coverage and site coverage was introduced through Eq. (4) (see Fig. 1).

A. Ideal clathrate hydrates

We start studying a system where lateral interactions were completely eliminated ($w_{m,n}/k_BT = 0.0$). In this ideal clathrate hydrate, only excluded volume interactions are considered and the spatial arrangement of molecules governs the adsorption process. Under these conditions, we performed Monte Carlo simulations using the scheme introduced in Sec. II A, and cluster analytical approximations according to Sec. II B. Then, the results obtained from CA were compared with the 2D clathrate hydrates (for species CH_4 and CO_2) simulations. In the framework of the inter- and intraspecies null lateral interactions, we shall demonstrate that CA can provide highly relevant information by allowing the description of 2D clathrate hydrates. Figures 3(a) and 4(a) show the behavior of the adsorption isotherms (θ_{cavity} versus $\beta\mu$) for each species. In both cases, an excellent agreement is found between CA and MC simulations. This finding suggests that the size and the geometry of the spatial arrangement in Fig. 2 perfectly capture the essence of the macroscopic sI structure.

In the case of methane [Fig. 3(a)], CA and MC adsorption isotherms demonstrate a remarkable qualitative and quantitative agreement across the entire chemical potential range. On the other hand, for carbon dioxide [Fig. 4(a)], the MC curve deviates slightly from the CA curve at intermediate coverage. For both species, the stability condition occurs when $\theta_{\text{cavity}} \approx 1.0$ (one molecule per cavity). $\theta_{\text{cavity}} > 1.0$ signifies multiple-cavity occupancy. The one molecule per cavity condition has been considered by different authors when calculating stability points and developing phase diagrams [22,23,27,33,50].

Furthermore, the cavity occupancy mechanism is reflected in the shape of the adsorption curves for each species. In the

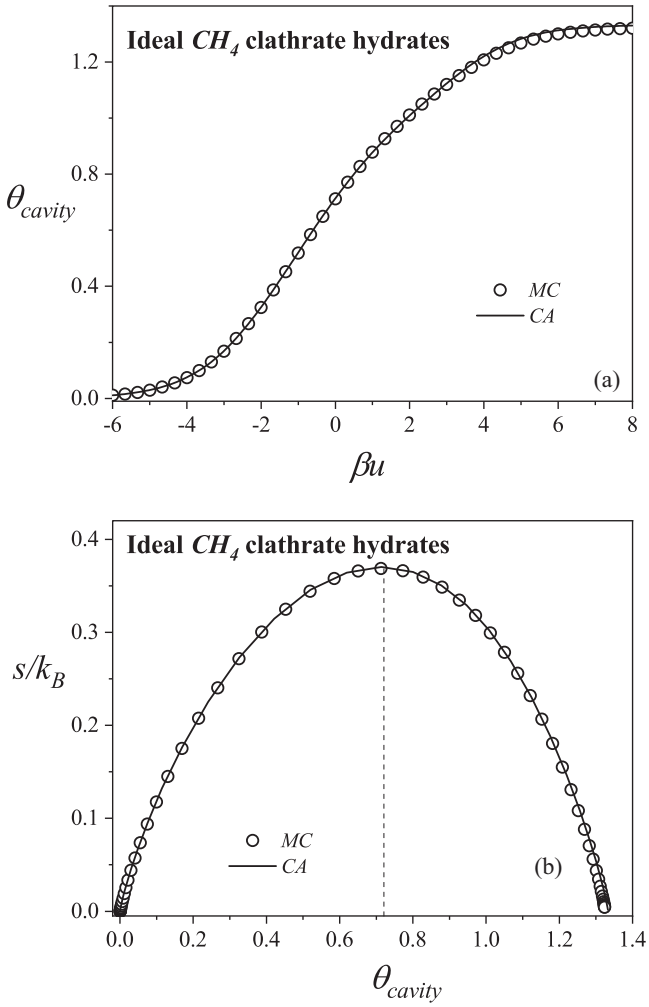

FIG. 3. Adsorption isotherm (a) and configurational entropy of the adsorbed phase versus coverage (b) for ideal CH_4 clathrate hydrates. Open circles represent MC data and solid lines correspond to CA results. In both cases, the lateral interactions were eliminated.

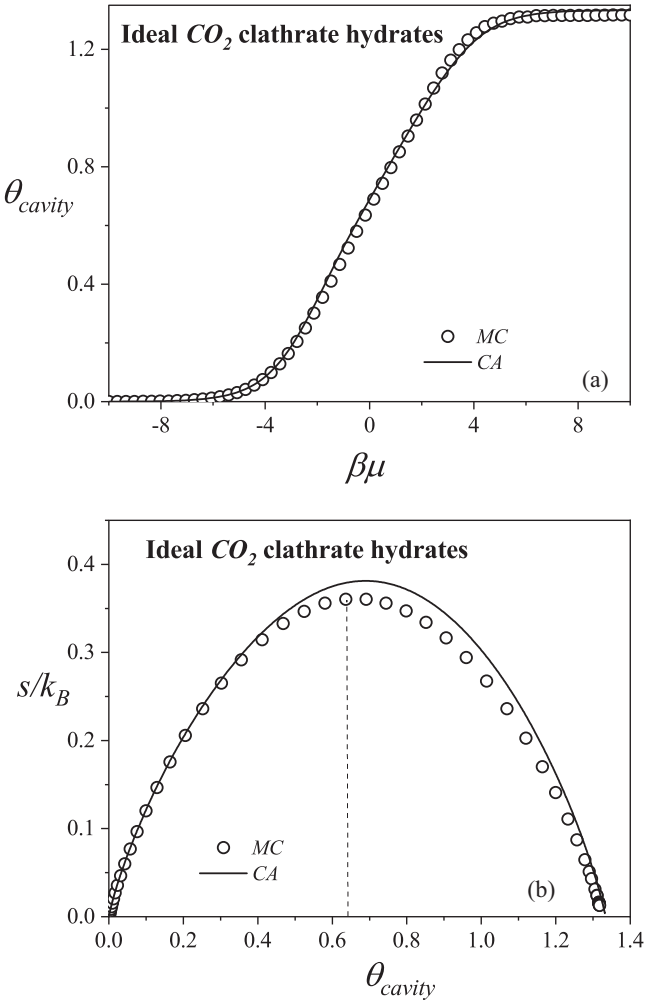

FIG. 4. Same as Fig. 3, but for ideal CO_2 clathrate hydrates.

case of methane, the corresponding adsorption isotherm tends to $\theta_{\text{cavity}} \approx 1.0$ following a Langmuir-type behavior. In this range of chemical potential ($\beta\mu = -6$ to 1.6), the methane coverage is lower than that corresponding to carbon dioxide. Due to its shape and size, methane is adsorbed in both large and small cavities without any discernible distinction between them. This behavior aligns with observations made by Glavatski and coworkers [45]. Conversely, for carbon dioxide, the adsorption isotherm requires a wider range of chemical potential ($\beta\mu = -6$ to 2.3) in order to reach a coverage of $\theta_{\text{cavity}} \approx 1.0$. The representation of carbon dioxide as the multiple occupancy of three consecutive sites in a straight line, with three directions and six possible orientations on the lattice, further contributes to its greater excluded volume interaction compared with methane as the cavity occupancy increases (very close to one molecule per cavity).

On the other hand, in Figs. 3(b) and 4(b), a comparative study for the configurational entropy per site as a function of cavity coverage is shown. In the case of the CA, entropy calculations are performed using Eq. (21). For MC simulations, the entropy was obtained through thermodynamic integration using Eq. (11). In Fig. 3(b) (CH_4 case), an excellent qualitative and quantitative agreement is found for the entropy calculated by CA and MC techniques. For the CO_2 case [Fig. 4(b)], the entropy for the CA model deviates slightly in a range of coverage where it approaches the maximum entropy value. This result is reasonable since the adsorption isotherm [Fig. 3(a)] also shows a slight deviation (in the same coverage range) compared with the MC simulations. For the CA theory, counting the states of linear trimers becomes more expensive in a coverage range between 0.65 and 1.1. In this range of cavity coverage, the CA system is further hindered by monomers that represent the sI structure. These monomers create obstacles that limit the efficiency of the CA system, resulting in an excessive count of states and preventing it from reaching values similar to those obtained in MC simulations. These discrepancies will be addressed in future studies by increasing the size of the cluster for the 2D CO_2 hydrate.

The curves of entropy in Figs. 3(b) and 4(b) exhibit their maxima within a narrow range of cavity coverage, specifically from 64% to 72%. For CO_2, the maximum entropy is closer to 64%. In our 2D lattice gas model [33], there is one small cavity for every two large cavities. This implies that approximately 66% of the vacant sites correspond to large cavities,

while the remaining 34% correspond to small cavities. It is likely that CO_2 occupies the large cavities at the entropy maximum due to the availability of more space and a greater number of possible arrangements, which enables the maximization of microstates within the cavity at a lower cost of adsorbed species. Conversely, CH_4 entropy maximum occurs towards the higher end of the range, around 72% cavity coverage, indicating that CH_4 maximizes its entropy by utilizing both large and small cavities without distinction, along with a higher percentage of adsorbed species. In the case of ideal clathrate hydrates, the maximization of entropy is equivalent to minimizing free energy ($f\beta = -s/k_B$). In terms of the stability behavior of hydrate clathrates, these findings suggest that CO_2 stabilizes more rapidly than CH_4 by exerting an entropic force that surpasses methane. Therefore, it is crucial to consider the excluded volume behavior by incorporating the CA theory with multiple-site occupancy for the guest species in the study of hydrate clathrate formation. This approach provides valuable insights into the evolution of these systems and offers important information for understanding their behavior.

B. Real clathrate hydrates

In this section, we present the results obtained for real (or interacting) hydrate clathrates. The lateral interactions (attractive) are introduced using the Lorentz-Berthelot rule [Eq. (2)] and expressed in units of $\beta = (k_BT)^{-1}$.

In Fig. 5, the adsorption isotherms [Fig. 5(a)] and the adsorption energies per site [Fig. 5(b)] are presented for CH_4 clathrate hydrates and two different temperatures: 200 and 298 K. The corresponding lateral interactions are as follows: $w_{1,1}/k_BT = -0.25$ (CH_4-CH_4) and $w_{1,2}/k_BT = -0.21$ (H_2O-CH_4) for 200 K; $w_{1,1}/k_BT = -0.17$ (CH_4-CH_4) and $w_{1,2}/k_BT = -0.14$ (H_2O-CH_4) for 298 K. Symbols and lines represent MC and CA results, respectively.

For both curves shown in Fig. 5(a), the coverage increases monotonically as the chemical potential (or equivalently, pressure) rises. It reaches the point of one molecule per cavity and eventually saturates at a state of multiple cavity occupancy at high chemical potential [45]. On the other hand, the energy per site [see Fig. 5(b)] decreases as the cavity coverage increases. Furthermore, as the temperature decreases, the lateral interactions between guest molecules and guest-water molecules become significant and have a marked influence on the energetic structure of the hydrate. Consequently, as seen in Fig. 5(b), lower temperatures correspond to higher energy for the sI structure and guest species across the entire range of cavity coverage.

Notably, the CA theory exhibits an excellent agreement with MC simulations for both the adsorption isotherms and energy curves. This comparison highlights the significant potential of CA in the field of statistical thermodynamics for real clathrate hydrates. The theory enables precise counting of the configurational factor $g_k(E_k)$ and the nearest-neighbor lateral interactions in all range of coverage. For real hydrates, unlike the ideal case, the CA factor Ξ_k is influenced by the spatial distribution of CH_4 guest species and the magnitude of the nearest-neighbor lateral interactions.

Moving on to CO_2 clathrate hydrates, Fig. 6 shows the adsorption isotherms [Fig. 6(a)] and the adsorption energies per

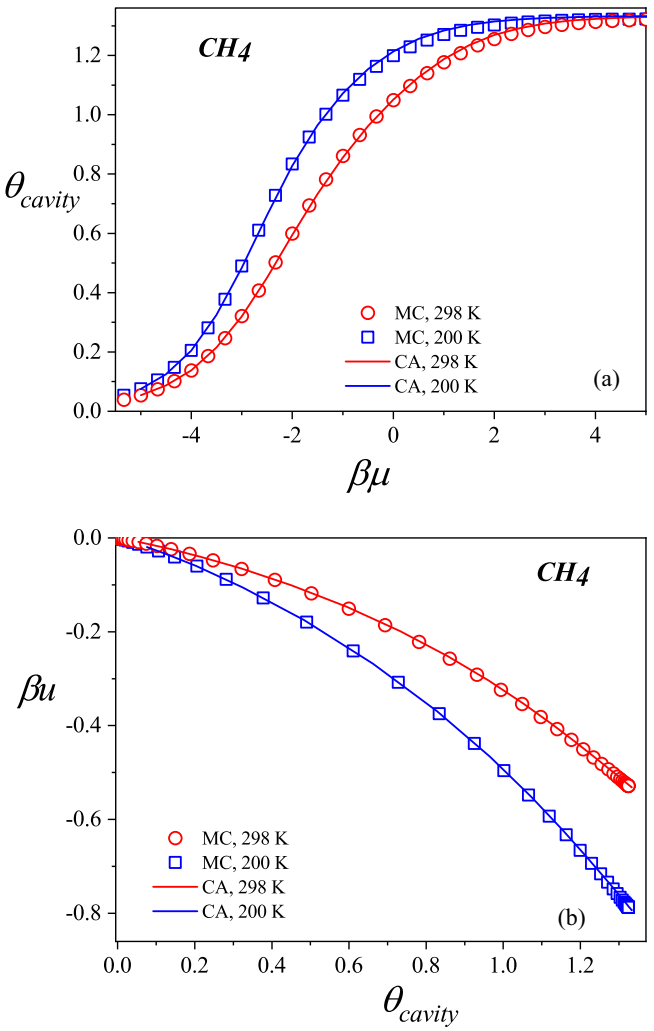

FIG. 5. (a) Adsorption isotherms and (b) adsorption energies per site (in k_BT units) versus cavity coverage for CH_4 clathrate hydrates and two different temperatures: 200 and 298 K. Symbols and solid lines correspond to MC and CA data, respectively: squares, 200 K; circles, 298 K; blue lines, 200 K; red lines, 298 K. In all cases, the lateral interactions were determined by using Eq. (2).

site [Fig. 6(b)] for $T = 220$ K and $T = 287$ K. In this case, the lateral interactions result in $w_{1,1}/k_BT = -0.35$ (CO_2-CO_2) and $w_{1,2}/k_BT = -0.23$ (H_2O-CO_2) for 220 K; $w_{1,1}/k_BT = -0.28$ (CO_2-CO_2) and $w_{1,2}/k_BT = -0.19$ (H_2O-CO_2) for 287 K. Symbols and solid lines correspond to MC and CA data, respectively. The behavior of the curves in Fig. 6 is similar to that discussed in Fig. 5. As in the previous figure, a good agreement is observed between CA and MC results. However, a slight deviation between theoretical and simulation data is observed in the adsorption isotherm at high coverage regime ($\theta_{\text{cavity}} > 1.0$). Under these conditions, linear CO_2 molecules confined in interacting hexagon chains lead to an expensive state-counting process. The small differences found in Fig. 6(a) are not observed in the case of Fig. 6(b).

Next, we examine the behavior of the heat of adsorption (q_d) as a function of cavity coverage at a temperature of 278 K (see Fig. 7). The adsorption heat, also known as encapsulation heat, was calculated using Eq. (6) (MC simulations,

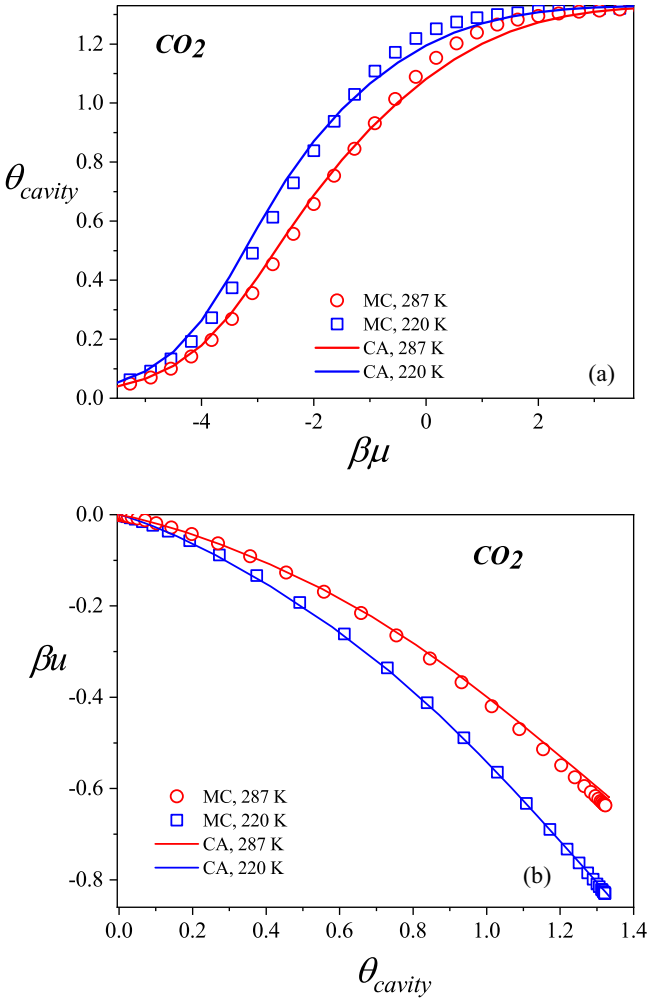

FIG. 6. (a) Adsorption isotherms and (b) adsorption energies per site (in k_BT units) versus cavity coverage for CO_2 clathrate hydrates and two different temperatures: 220 and 287 K. Symbols and solid lines correspond to MC and CA data, respectively: squares, 220 K; circles, 287 K; blue lines, 220 K; red lines, 287 K. In all cases, the lateral interactions were determined by using Eq. (2).

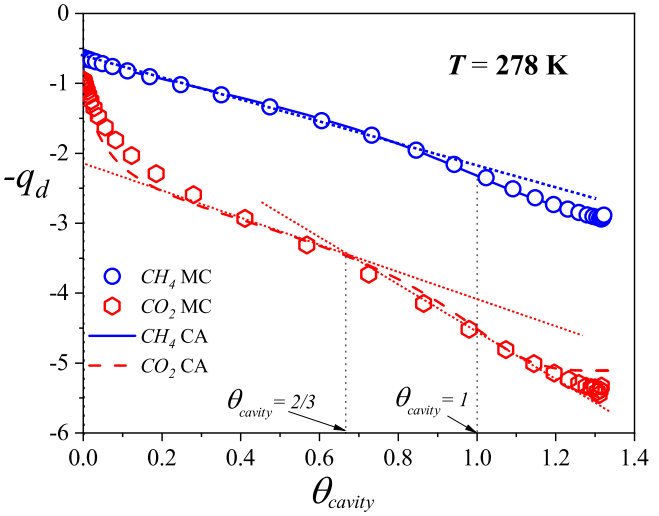

FIG. 7. Negative heat of adsorption versus cavity coverage for CH_4 and CO_2 clathrate hydrates. Symbols and solid lines correspond to MC and CA data, respectively: circles and solid line (CH_4); and hexagons and dashed line (CO_2). The curves were obtained for $T = 278$ K. The lateral interactions were determined by using Eq. (2).

symbols) and Eq. (17) (CA theory, lines). Circles (hexagons) and solid (dashed) line represent results obtained for CH_4 (CO_2) clathrate hydrates. As in Refs. [45,71], the negative value of the adsorption heat is analyzed. The function $q_d(\theta_{\text{cavity}})$ offers a fundamental tool for studying the occupancy behavior and cavity preference in clathrate hydrates with different guest species [45,71,72].

The negative value of the adsorption heat for the case of CH_4 guest species decreases almost linearly (with increasing chemical potential) in the cavity filling range between 0 and approximately 0.97 ($0.0 < \theta_{\text{cavity}} < 0.97$). The linear behavior of this curve indicates that CH_4 does not distinguish between small and large cavities during clathrate formation. This behavior has been previously observed by Glavatskiy *et al.* [45]. However, above one molecule per cavity, the curve deviates from linearity due to multiple-site occupancy, and the system becomes more unstable in the high-chemical-potential range. On the other hand, CO_2 exhibits two distinct regions for $-q_d$ throughout the entire cavity coverage range. Firstly, at low coverage ($0.0 < \theta_{\text{cavity}} < 0.11$), $-q_d$ decreases abruptly due to both the strong interactions (CO_2-H_2O) and the size ratio between CO_2 and the water molecules that form the large cavities. Subsequently, this curve stabilizes into a straight line with a steeper slope compared to CH_4, within the same coverage range. This phenomenon occurs in the range of large cavity occupancy (first region, between $\theta_{\text{cavity}} \approx 0.0$ and approximately $\theta_{\text{cavity}} \approx 2/3$) because the size of CO_2 is almost double that of CH_4 [44]. As a result, CO_2 has a preference for occupying larger cavities to achieve greater comfort within the cavity and enhance stability. Above $\theta_{\text{cavity}} \approx 2/3$, a change in the slope of the curve is observed towards a more negative slope, corresponding to the occupancy of small cavities in the hydrate (second region). In this region, CO_2 molecules are encapsulated in the smaller cavities of sI, but in a much less comfortable manner compared to the first region. The CA theory model has the advantage of highlighting the changes in the slopes of $-q_d$ as different types of cavities in sI are filled, providing insights into the occupancy states and preferences of guest species (CO_2 and CH_4).

To conclude with the analysis of Fig. 7, it is important to remark that an excellent qualitative and quantitative agreement is observed between CA theory and MC simulations. The CA theory also offers the advantage of highlighting changes in the slopes of $-q_d$ as different types of cavities in sI are filled, providing insights into the occupancy states and preferences of guest species (CO_2 and CH_4). In the case of CH_4 molecules, a high level of agreement can be observed across the entire range of cavity coverage. Conversely, for CO_2 guest species, there is a slight quantitative discrepancy at low cavity coverage and at very high coverage where multiple cavity occupancy occurs. This slight discrepancy with our CA model is associated with the fact that our CA model does not consider cavity distortion and, therefore, the flexibility of the sI structure. Introducing the flexibility phenomenon into the

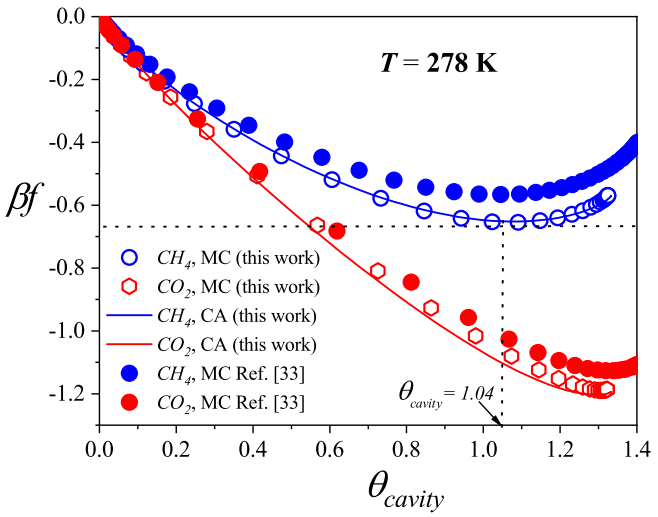

FIG. 8. Free energy per site (in k_BT units) versus cavity coverage for CO_2 (red hexagons, red lines) and CH_4 (blue circles, blue lines) clathrate hydrates. The curves have been obtained for $T = 278$ K. Symbols represent MC simulations and lines correspond to CA results. The figure also includes MC simulation curves obtained considering the possible distortion of the cavities [33].

CA theoretical model for the 2D hydrate structure remains an objective for future work.

We now continue with the study of the free energy per site [Eqs. (10) and (23)]. In Fig. 8, we present the comparison between CA theory (lines) and MC simulations (symbols) for the free energy per site (in k_BT units) as a function of cavity coverage for both guest species, CH_4 and CO_2. The curves have been obtained for $T = 278$ K.

The free-energy curve for CH_4 exhibits a nonmonotonic dependence on cavity coverage. It decreases within the range $0 \leqslant \theta_{\text{cavity}} < 1$, reaches a minimum at approximately $\theta_{\text{cavity}} = 1.0$, and, subsequently, as the cavity occupancy exceeds 1 ($\theta_{\text{cavity}} > 1.0$), the free energy experiences a slight increase, indicating high instability resulting from multiple cavity occupancy. The minimum at $\theta_{\text{cavity}} \approx 1.0$ signifies the presence of one molecule per cavity and represents the state of maximum stability within the clathrate hydrate system [22,23,27,33,50].

While this study did not account for the distortion of cavities in the sI structure, the results obtained here are in agreement with those from our previous work [33] that employed MC simulations with distorted cavities (flexible sI structure).[1] In Ref. [33], we found that the free-energy minimum at $\theta_{\text{cavity}} \approx 1.0$ coincides with a minimum in cavity deformation, indicating the highest level of system stability. In other words, both cavity distortion and the spatial distribution of CH_4 species in relation to water molecules contribute to the free-energy minimum at $\theta_{\text{cavity}} \approx 1.0$. The solid symbols in Fig. 8 represent the free energy per site calculated using flexible 2D MC simulations at 278 K, as reported in Ref. [33]. Based on these findings, we can deduce that, in the case of a fixed structure (or frozen structure), CH_4 molecules redistribute to adopt the configuration shown in Fig. 1(b), thereby stabilizing the sI clathrate hydrate at $\theta_{\text{cavity}} \approx 1.0$.

Enforcing the constraint of fixing the sI structure results in a specific arrangement of CH_4 molecules, which, in turn, leads to a deeper minimum in the free energy compared to the flexible structure. As a result, CH_4 species have the potential to achieve stabilization without the need for distorting the sI structure. This finding aligns with studies conducted by Henley *et al.* [73], who employed the constant-pressure Gibbs ensemble MC method. Their research clearly indicates that the rigid clathrate hydrate model provides a more accurate prediction of cavity occupancy within the experimental data range when compared to flexible models.

In the case of carbon dioxide molecules, the function $\beta f(\theta_{\text{cavity}})$ decreases abruptly towards more negative values as the cavities are filled. This decrease indicates a greater level of stability compared to methane hydrate. The minimum of the free-energy curve is found at $\theta_{\text{cavity}} \approx 1.3$ (rather than $\theta_{\text{cavity}} \approx 1.0$), shifted to the right in regions where multiple cavity occupancy occurs. This behavior can be attributed to the preference of CO_2 molecules for larger cavities [2,6,74–76]. Consequently, as observed in previous works [45], at very high chemical potentials, CO_2 molecules can be repositioned in pairs within a large cavity.

Figure 8 also includes the simulation free energy curve obtained in Ref. [33] for 2D flexible clathrate hydrates (represented by the dashed red line). A comparison reveals that the free energy of the flexible clathrate hydrate is higher than that of the frozen hydrate. While cavity distortions play a crucial role in the encapsulation process, our study demonstrates that flexible CO_2 sI hydrate exhibits slightly lower stability than the fixed structure. The physical behavior of cavity distortion or deformation results in a minor reduction in the stability of the clathrate hydrate for the CO_2 guest species.

As in Figs. 3–5, we observe excellent agreement between theory and simulation for CH_4 sI clathrate hydrates. In this case, the CA model with a cluster size of 4×10 has proven to be sufficiently representative for describing the 2D clathrate hydrate [33–35]. For CO_2 guest species, a slight discrepancy between theory and simulation is found. Future work will focus on developing a more efficient counting method for CO_2 states and increasing the size of the calculation cell. With these improvements, we aim to calculate a configurational factor that aligns more closely with the system's symmetry in the CA model and further enhance the agreement between theoretical predictions and CA simulation results.

The results obtained in Secs. III A and III B validate the theoretical methodology used in this work, highlighting

[1] In general, it has been proven through experiments and simulations that the structure of clathrate hydrates undergoes cavity distortion [31,32,46,50]. That is, the cavities expand and contract when the guest species is inside them. This phenomenon of distortion observed in the experiment was introduced in the study of Ref. [33], allowing the displacement of the H_2O molecules and *O* sites (see Fig. 1) to neighboring sites. Accordingly, the level of distortion was measured as the ratio between the number of H_2O molecules and *O* sites that move from their original locations and the total number of H_2O molecules and *O* sites forming the sI structure without deformation. The displacement of the H_2O molecules and *O* sites modifies the size of the cavities and affects the stability of the system.

the future potential of the CA theory to describe the thermodynamic behavior of clathrate hydrates in higher spatial dimensions.

C. Clathrate hydrates in the presence of repulsive lateral interactions

In this section, the case of repulsive lateral interactions ($w_{m,n}/k_BT > 0$) is considered. This strategy can be an effective way to introduce steric hindrance in the system, offering insights into the occupancy state of cavities within the hydrate clathrate structure. Rodger [77,78] suggested that guest repulsion is more pivotal than attraction in maintaining cavity expansion and, consequently, the existence of the cavity itself. Here, we perform an exhaustive analysis of adsorption isotherms and energies of the adsorbed phase using CA theory and MC simulations within the context of exclusively repulsive lateral interactions. The objective is to scrutinize the occupation relationships of the different cavities by the corresponding guest species (CO_2 and CH_4) [79–83]. We consider the water-guest lateral interaction to be stronger than the guest-guest lateral interaction ($w_{1,2}/k_BT > w_{1,1}/k_BT > 0$). In addition, the water-water interactions are assumed to be zero ($w_{2,2}/k_BT = 0$, no distortion is considered).

We start by studying the case of CH_4 clathrate hydrates, see Fig. 9. In Fig. 9(a), the adsorption isotherms are presented for different values of the lateral interactions, as indicated in the inset. The corresponding curves of the adsorption energy are shown in Fig. 9(b). Symbols and solid lines correspond to MC and CA data, respectively. In Fig. 10, the study is repeated for CO_2 clathrate hydrates.

Firstly, let us examine the behavior of the adsorption isotherms for CH_4 [Fig. 9(a)] and CO_2 [Fig. 10(a)] species. In both instances, as repulsive interactions increase, the isotherms shift towards higher values of chemical potential. However, notable distinctions emerge in the shapes of the curves corresponding to each species (CH_4/CO_2). In each figure, the ideal case where lateral interactions are absent is included for reference purposes.

For CH_4 guest molecules, the adsorption isotherms exhibit the emergence of a plateau as the repulsion between water molecules and CH_4 species intensifies, particularly around the value of $\theta_{\text{cavity}} \approx 1.0$. When a strong H_2O-CH_4 interaction is taken into account, the plateau becomes clearly visible in the adsorption isotherm. As an illustrative example, Fig. 9(a) depicts the case where $w_{1,2}/k_BT = +1.0$ and $w_{1,1}/k_BT = 0.0$ (represented by open down triangles) and the case where $w_{1,2}/k_BT = +2.0$ and $w_{1,1}/k_BT = 0.0$ (represented by dot-dashed line). As the plateau is reached, each cavity is occupied by a single molecule. Furthermore, only one adsorption regime is observed for θ_{cavity} ranging from zero to one. In terms of cavity occupancy, this finding suggests that the CH_4 molecules do not differentiate between large and small cavities as they adsorb with increasing chemical potential. This behavior can be attributed to the size and shape of the CH_4 molecules in relation to the sizes of the cavities.

On the other hand, the adsorption isotherms for CO_2 also exhibit the emergence of plateaus as the repulsion between water and guest molecules intensifies [see Fig. 10(a)]. However, unlike the case of methane, the plateau starts to become

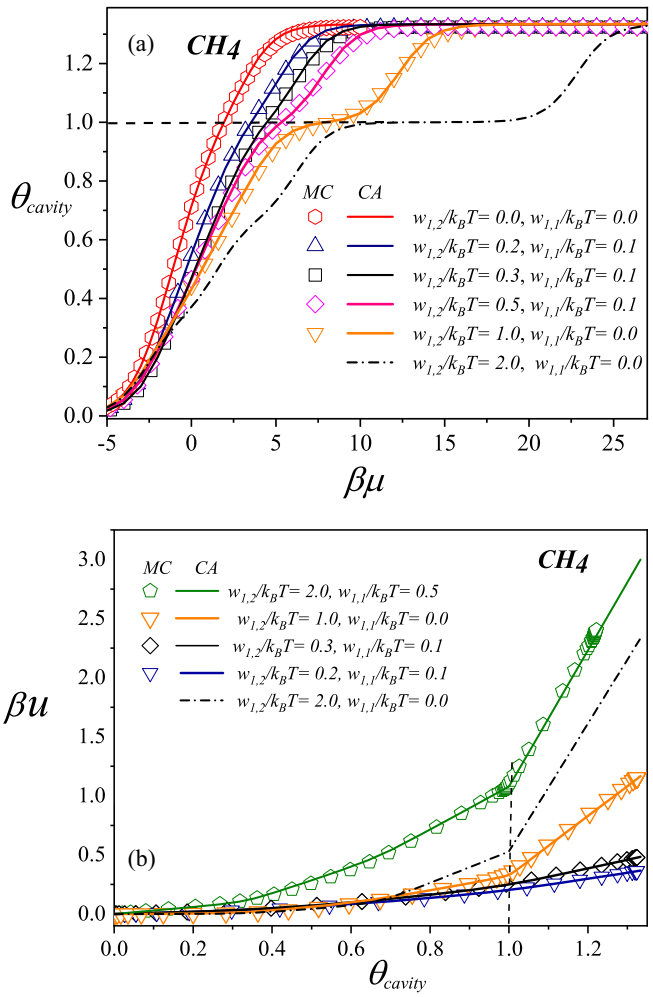

FIG. 9. (a) Adsorption isotherms and (b) adsorption energies per site (in k_BT units) versus cavity coverage for CH_4 clathrate hydrates and different values of $w_{m,n}/k_BT$ as indicated. Symbols and solid lines correspond to MC and CA data, respectively. For the case of $w_{1,2}/k_BT = +2.0$ [the strongest interaction considered in panel (a)], MC simulations are highly demanding and only the results corresponding to CA theory are presented (dot-dashed line).

noticeable at $\theta_{\text{cavity}} \approx 2/3$. The singularity is particularly evident in the case of $w_{1,2}/k_BT = +2.0$ and $w_{1,1}/k_BT = 0.0$ (represented by the dot-dashed line in the figure), separating two clearly distinguishable adsorption regimes: (i) the first regime occurs at cavity coverage between zero and 2/3, primarily associated with the filling of large cavities; and (ii) the second regime begins with the occupation of small cavities and continues until saturation, leading to multiple cavity occupancy for $\theta_{\text{cavity}} > 1.0$. Overall, the insights from Figs. 9(a) and 10(a) shed light on the increasing significance of steric hindrance (repulsive interactions). This concept provides a valuable tool for understanding the formation of sI hydrate clathrates in the case of species like CH_4 and CO_2, enabling us to draw conclusions about cavity occupancy processes as chemical potential increases.

Another complementary approach to investigate state occupancy involves examining adsorption energies as a function of cavity coverage [see Figs. 9(b) and 10(b)]. For both CH_4

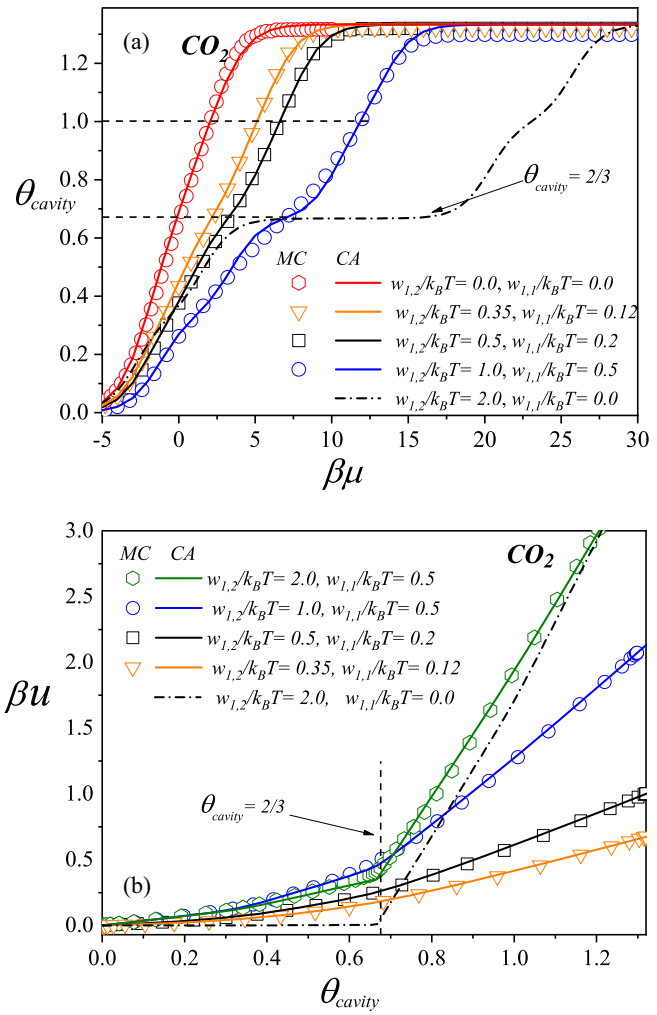

FIG. 10. Same as Fig. 9 but for CO_2 clathrate hydrates. For the case of $w_{1,2}/k_BT = +2.0$ [the strongest interaction considered in panel (a)], MC simulations are highly demanding and only the results corresponding to CA theory are presented (dot-dashed line).

and CO_2, a gradual increase in adsorption energy becomes evident as cavity occupancy develops, particularly when weak repulsive interactions are present across the entire range of coverage. In cases of strong repulsive interactions, such as $w_{1,2}/k_BT = +2.0$ ($w_{2,2/k_BT} = +0.5$) for CH_4, as well as $w_{1,2}/k_BT = +1.0$ ($w_{2,2/k_BT} = +0.5$) for CO_2, the curves exhibit a sudden transition characterized by a change in the slope of the energy curves at $\theta_{\text{cavity}} \approx 1.0$ for CH_4 and $\theta_{\text{cavity}} \approx 2/3$ for CO_2.

The observations from the previous paragraph reveal a distinct pattern of occupancy preference, which is similar to what was observed in the earlier adsorption isotherms, as illustrated in Figs. 9(a) and 10(a). Specifically, for CH_4 molecules, there is a sudden change in energy starting at $\theta_{\text{cavity}} \approx 1.0$. For $\theta_{\text{cavity}} < 1$, the energy curves exhibit a monotonic increase, suggesting that the size ratio between the cavity and guest molecule is not a determining factor (there is no distinction between large and small cavities in the filling process). In contrast, the analysis of CO_2 suggests a distinction in the size ratio between the cavity and guest molecule. CO_2 shows a preference for occupying the larger cavities within the sI structure. According to the Kihara potential parameters [51], the core radius of a CO_2 molecule is approximately twice that of a CH_4 molecule. This physical phenomenon becomes evident around $\theta_{\text{cavity}} \approx 2/3$, where a distinct increase in repulsive energy indicates the insertion of CO_2 guests into the smaller cavities of the sI clathrate structure.

We now analyze the behavior of the theoretical approximation. As it can be observed from Figs. 9 and 10, a remarkable qualitative and quantitative agreement between CA and MC results becomes evident across the spectrum of chemical potentials and cavity coverage for both adsorption isotherms and adsorption energies. For the CO_2 guest species, a slight discrepancy emerges at intermediate coverage between CA theory and MC simulations when lateral interactions are exceptionally strong. Under these conditions, MC simulations are highly demanding because the relaxation time increases very fast with the magnitude of the lateral couplings. The results presented in Figs. 9 and 10 underscore the considerable promise of the CA approach for investigating clathrate hydrates and their filling mechanisms.

In Sec. III, the study was conducted within the framework of the CA theoretical model and was complemented by MC simulations to validate our results. This approach allowed us to develop a comprehensive theory-simulation study, yielding more robust results for calculating thermodynamic functions in 2D sI clathrate hydrates. In future research, we plan to (1) complement our theoretical analysis with molecular dynamics (MD) and density-functional theory (DFT) calculations, (2) incorporate the study of fluctuations in our coarse-grained model using the recently introduced molecular dynamics lattice gas approach [84–86], and (3) compare our predictions with experimental data from the literature.

IV. CONCLUSIONS

This study has focused on exploring of thermodynamic properties in a two-dimensional rigid clathrate hydrate system that includes CH_4 and CO_2 guest molecules. The investigation employed a 2D lattice-gas model combined with MC simulations and CA analytical calculations, which involve exact counting of states within small cells. The validity and reliability of the research were verified by quantitative and qualitative comparisons between theoretical and simulation data.

The CA model has displayed significant potential in characterizing clathrate hydrates. It serves as a valuable complementary theoretical tool alongside MC simulations, and the synergy between the two methodologies enhances their analytical capabilities. Based on these explorations, the key findings of this study can be divided into two main categories. The first category involves validating CA for studying hydrate clathrates. This task was carried out in two stages (ideal and real hydrate clathrates):

(1) The model introduced in Sec. II offers a 2D simplification of real clathrates aimed at providing deeper insight into the physical interactions and excluded volume effects between the sI structure and its host molecules. The triangular lattice, with connectivity = 6, highlights the minimum number of neighbors required to understand occupancy behavior, stability, and structural distortions. The excluded volume

effect, which is critical in these complex systems, is effectively addressed using a lattice-gas model with multiple-site occupancy. This approach has been validated across various complex systems, including studies on surface phenomena [64], ferromagnetism [87,88], liquid crystals [89], phase transitions [90], and critical phenomena [91].

(2) Regarding ideal hydrate clathrates, the CA theory and MC simulations showed good agreement in comparisons of adsorption isotherms and configurational entropy of the adsorbed phase. In the case of CO_2 guest species, a slight discrepancy was observed in the filling of small cavities. The formation of hydrate clathrates in the absence of energetic interactions is governed by excluded-volume interactions and the spatial arrangement of molecules. These qualitative and quantitative agreements suggest that the CA theory is highly valuable in understanding the role of excluded-volume interactions during clathrate hydrate formation.

(3) In the case of real hydrate clathrates with genuine energetic interactions, an excellent agreement between the CA theory and MC simulations was observed for various thermodynamic functions, including adsorption isotherms, adsorption energies, heat of adsorption, and the free energy of the 2D hydrate clathrate system. Calculating the heat of adsorption (q_d) allowed for an analysis of preferential adsorption behavior in cavities filled with CO_2 and CH_4. Additionally, free energy comparisons between CA and MC simulations were conducted for fixed and distorted cavity structures. The results indicated that CH_4 species can stabilize the hydrate without distorting the sI structure, while flexible sI CO_2 hydrate exhibited slightly lower stability. Cavity deformation reduced the stability of CO_2 hydrates.

The results obtained for ideal and real systems illustrate the potential of CA theory as an innovative tool for future studies on hydrate clathrate occupancy. The second category involves new findings demonstrating the value of including repulsive lateral interactions between guest molecules in studying sI hydrate clathrate formation and cavity occupancy processes. The repulsive couplings prove to be an effective way to introduce steric hindrance in the system.

Finally, it should be mentioned that a comprehensive analysis of the clathrate hydrate problem is quite challenging due to the complexity of the involved systems. Thus, the lattice-gas model presented here can be considered an initial coarse-grained approach, serving as a starting point for addressing clathrate hydrate phase equilibria. Our approach may not be as accurate as MD simulations and DFT calculations, but it is elegant, computationally inexpensive and, with slight modifications, could be applied to other related areas such as adsorption in zeolites and metal-organic frameworks. Moreover, given that this is a problem with a large number of variables, the development of simplified models like the one introduced here contributes to a better analysis of the obtained results. If this perspective is complemented with more sophisticated developments such as MD and DFT, the understanding of the problem is enriched. Additionally, the application of the CA approach allows us to identify and characterize the most prominent features of complex phenomena such as cavity occupancy and selectivity in terms of the microscopic properties of the system [configurational factor $g_k(E_k)$, Eq. (13)]. This has great potential for studying the possible existence of phase transitions or structural changes under different thermodynamic conditions. Studies in this line are in progress, and they involve the combination of our simplified model with MD- and DFT-based calculation models.

ACKNOWLEDGMENTS

This work was supported in part by CONICET (Argentina) under Project No. PIP 11220220100238CO; Universidad Nacional de San Luis (Argentina) under Project No. 03-0816; and the National Agency of Scientific and Technological Promotion (Argentina) under project PICT-2013-1678. The numerical work were done using the BACO parallel cluster [92] located at Instituto de Física Aplicada, Universidad Nacional de San Luis - CONICET, San Luis, Argentina.

[1] E. D. Sloan and C. A. Koh, *Clathrate Hydrates of Natural Gases* (CRC Press, Boca Raton, 2008).
[2] E. D. Sloan, Jr., Nature (London) **426**, 353 (2003).
[3] M. von Stackelberg and H. R. Miller, Z. Elektrochem. **58**, 25 (1954).
[4] W. F. Claussen, J. Chem. Phys. **19**, 1425 (1951).
[5] L. Pauling and R. E. Marsh, Proc. Natl. Acad. Sci. USA **38**, 112 (1952).
[6] J. Ripmeester, J. Tse, C. Ratcliffe, and B. Powell, Nature (London) **325**, 135 (1987).
[7] K. A. Udachin, C. I. Ratcliffe, G. D. Enright, and J. A. Ripmeester, Supramol. Chem. **8**, 173 (1997).
[8] J. L. Atwood, J. E. D. Davies, and D. D. McNicol, *Inclusion Compounds* (Academic Press, London, 1984).
[9] G. A. Jeffrey and R. K. McMullan, Prog. Inorg. Chem. **8**, 43 (1967).
[10] D. Weaire and R. Phelan, Philos. Mag. Lett. **69**, 107 (1994).
[11] W. Thomson, Philos. Mag. **24**, 503 (1887).
[12] M. Lasich, Fluid Phase Equilib. **456**, 131 (2018).
[13] T. S. Collett, AAPG Bull **86**, 1971 (2002).
[14] M. R. Walsh, S. H. Hancock, S. Wilson, S. L. Patil, G. J. Moridis, R. Boswell, T. S. Collett, C. A. Koh, and E. D. Sloan, Energy Econ. **31**, 815 (2009).
[15] G. J. Moridis, T. S. Collett, R. Boswell, M. Kurihara, M. T. Reagan, C. A. Koh, and E. D. Sloan, SPE Reservoir Eval. Eng. **12**, 745 (2009).
[16] Y. F. Makogon, *Hydrates of Hydrocarbons* (Pennwel Publishing Company, Tulsa, 1997).
[17] S. G. Hatzikiriakos and P. Englezos, Chem. Eng. Sci. **48**, 3963 (1993).
[18] P. G. Brewer, Jr., G. Friederich, E. T. Peltzer, and F. M. Orr, Science **284**, 943 (1999).
[19] J. Javanmardi and M. Moshfegiam, Appl. Therm. Eng. **23**, 845 (2003).
[20] S. Thomas and R. A. Dawe, Energy **28**, 1461 (2003).

[21] A. A. Khokhar, J. S. Gudmundsson, and E. D. Sloan, Fluid Phase Equilib. **150**, 383 (1998).
[22] J. H. van der Waals and J. C. Platteeuw, Adv. Chem. Phys. **2**, 1 (1959).
[23] W. R. Parrish and J. M. Prausnitz, Ind. Eng. Chem. Proc. Des. Dev. **11**, 26 (1972).
[24] H. Tanaka, J. Chem. Phys. **101**, 10833 (1994).
[25] R. E. Westacott and M. P. Rodger, Chem. Phys. Lett. **262**, 47 (1996).
[26] H. Tanaka, T. Nakatsuka, and K. Koga, J. Chem. Phys. **121**, 5488 (2004).
[27] H. Pimpalgaonkar, S. K. Veesam, and S. N. Punnathanam, J. Phys. Chem. B **115**, 10018 (2011).
[28] N. I. Papadimitriou, I. N. Tsimpanogiannis, A. K. Stubos, A. Martín, L. J. Rovetto, L. J. Florusse, and C. J. Peters, J. Phys. Chem. B **115**, 1411 (2011).
[29] A. A. Chialvo, M. Houssa, and P. T. Cummings, J. Phys. Chem. B **106**, 442 (2002).
[30] S. J. Wierzchowski and P. A. Monson, J. Phys. Chem. B **111**, 7274 (2007).
[31] V. V. Sizov and M. E. Piotrovskaya, J. Phys. Chem. B **111**, 2886 (2007).
[32] S. R. Zele, S.-Y. Lee, and G. D. Holder, J. Phys. Chem. B **103**, 10250 (1999).
[33] P. Longone, A. Martín, and A. J. Ramirez-Pastor, Fluid Phase Equilib. **402**, 30 (2015).
[34] P. Longone, A. Martín, and A. J. Ramirez-Pastor, Fluid Phase Equilib. **521**, 112739 (2020).
[35] P. Longone, A. Martín, and A. J. Ramirez-Pastor, J. Phys. Chem. B **126**, 878 (2022).
[36] F. O. Sanchez-Varretti, G. D. Garcia, P. M. Pasinetti, and A. J. Ramirez-Pastor, Adsorption **20**, 855 (2014).
[37] F. O. Sanchez Varretti, F. Bulnes, and A. J. Ramirez-Pastor, Appl. Surf. Sci. **387**, 268 (2016).
[38] F. O. Sanchez-Varretti, P. M. Pasinetti, F. Bulnes, and A. J. Ramirez-Pastor, Adsorption **23**, 651 (2017).
[39] F. O. Sanchez-Varretti, F. Bulnes, and A. J. Ramirez-Pastor, Physica A **518**, 145 (2019).
[40] N. M. De La Cruz Feliz Cruz Feliz, P. J. Longone, F. O. Sanchez-Varretti, F. Bulnes, and A. J. Ramirez-Pastor, Phys. Chem. Chem. Phys. **25**, 14942 (2023).
[41] F. O. Sanchez-Varretti, E. V. Gómez, L. B. Avalle, F. M. Bulnes, M. C. Gimenez, and A. J. Ramirez-Pastor, Appl. Surf. Sci. **500**, 144034 (2020).
[42] F. O. Sanchez-Varretti, P. M. Pasinetti, F. M. Bulnes, and A. J. Ramirez-Pastor, Surf. Sci. **701**, 121698 (2020).
[43] F. O. Sanchez-Varretti, F. M. Bulnes, and A. J. Ramirez-Pastor, Eur. Phys. J. E **44**, 42 (2021).
[44] R. T. Morrison and R. N. Boyd, *Organic Chemistry* (Prentice-Hall International, New Jersey, 1992).
[45] K. S. Glavatskiy, T. J. H. Vlugt, and S. J. Kjelstrup, J. Phys. Chem. B **116**, 3745 (2012).
[46] M. Lasich, A. H. Mohammadia, K. Bolton, J. Vrabec, and D. Ramjugernath, Fluid Phase Equilib. **369**, 47 (2014).
[47] H. A. Lorentz, Ann. Phys. **248**, 127 (1881).
[48] H. A. Lorentz, Ann. Phys. **248**, 660 (1881).
[49] D. Berthelot, Compt. Rend. Acad. Sci. **126**, 1 (1898).
[50] A. Martín and C. J. Peters, J. Phys. Chem. C **113**, 422 (2009).
[51] L. S. Tee, S. Gotoh, and W. E. Stewart, Ind. Eng. Chem. Fund. **5**, 363 (1966).
[52] D. Nicholson and N. G. Parsonage, *Computer Simulation and the Statistical Mechanics of Adsorption* (Academic, London, 1982).
[53] J. E. González, A. J. Ramirez-Pastor, and V. D. Pereyra, Langmuir **17**, 6974 (2001).
[54] F. Romá, J. L. Riccardo, and A. J. Ramirez-Pastor, Langmuir **21**, 2454 (2005).
[55] N. Metropolis, A. W. Rosenbluth, M. N. Rosenbluth, A. H. Teller, and E. Teller, J. Chem. Phys. **21**, 1087 (1953).
[56] V. A. Bakaev and W. A. Steele, Langmuir **8**, 148 (1992).
[57] K. Binder, *Applications of the Monte Carlo Method in Statistical Physics*, Topics in Current Physics Vol. 36 (Springer, Berlin, 1984).
[58] K. Binder, J. Stat. Phys. **24**, 69 (1981).
[59] T. L. Polgreen, Phys. Rev. B **29**, 1468 (1984).
[60] P. M. Pasinetti, A. J. Ramirez-Pastor, E. E. Vogel, and G. Saravia, Phys. Rev. E **104**, 054136 (2021).
[61] P. M. Pasinetti, A. J. Ramirez-Pastor, and E. E. Vogel, Phys. Rev. E **107**, 064126 (2023).
[62] J. P. Hansen and L. Verlet, Phys. Rev. **184**, 151 (1969).
[63] A. J. Ramirez-Pastor and F. Bulnes, Physica A **283**, 198 (2000).
[64] T. L. Hill, *An Introduction to Statistical Thermodynamics* (Addison-Wesley, Reading, MA, 1960).
[65] F. Farhang, A. V. Nguyen, and M. A. Hampton, Energ. Fuel. **28**, 1220 (2014).
[66] N. N. Nguyen and A. V. Nguyen, Fuel **156**, 87 (2015).
[67] H. Jia, F. Fan, Q. Wang, Z. Shen, Y. Wang, H. Sun, P. Pei, C. Li, K. Lv, and P. Huang, Langmuir **40**, 9012 (2024).
[68] X. Jing, Q. Luo, X. Cui, Q. Wang, Y. Liu, and Z. Fu, J. Mol. Liq. **366**, 120237 (2022).
[69] C. Sun and G. Chen, in *Proceedings of the 5th International Conference on Gas Hydrates (ICGH 2005), Trondheim, Norway* (Tapir Academic Press, Norway, 2005), pp. 201–207.
[70] Y. Chen, X. Zhou, C. Tang, X. Zang, J. Guan, J. Lu, and D. Liang, Chem. Eng. J. **498**, 155097 (2024).
[71] T. J. H. Vlugt, E. García-Pérez, D. Dubbeldam, S. Ban, and S. Calero, J. Chem. Theory Comput. **4**, 1107 (2008).
[72] A. Patt, J.-M. Simon, S. Picaud, and J. M. Salazar, J. Phys. Chem. C **122**, 18432 (2018).
[73] H. Henley and A. Lucia, J. Nat. Gas Sci. Eng. **26**, 446 (2015).
[74] A. Khan, J. Mol. Struct (THEOCHEM) **664-665**, 237 (2003).
[75] K. A. Udachin, C. I. Ratcliffe, and J. A. Ripmeester, J. Phys. Chem. B **105**, 4200 (2001).
[76] J. A. Ripmeester and C. I. Ratcliffe, J. Phys. Chem. **94**, 8773 (1990).
[77] P. M. Rodger, J. Phys. Chem. **94**, 6080 (1990).
[78] P. M. Rodger, Mol. Simul. **5**, 315 (1990).
[79] R. Sun and Z. Duan, Geochim. Cosmochim. Acta **69**, 4411 (2005).
[80] J. L. De Roo, C. J. Peters, R. N. Lichtenthaler, and G. A. M. Diepen, AIChE J. **29**, 651 (1983).
[81] T. J. Galloway, W. Ruska, P. S. Chappelear, and R. Kobayashi, Ind. Eng. Chem. Fund. **9**, 237 (1970).

[82] Y. P. Handa, J. Chem. Thermodyn. **18**, 915 (1986).
[83] J. B. Klauda and S. I. Sandler, J. Phys. Chem. B **106**, 5722 (2002).
[84] M. R. Parsa and A. J. Wagner, Phys. Rev. E **96**, 013314 (2017).
[85] T. Blommel and A. J. Wagner, Phys. Rev. E **97**, 023310 (2018).
[86] M. R. Parsa and A. J. Wagner, Phys. Rev. Lett. **124**, 234501 (2020).
[87] W. Lenz, Phys. Z. **21**, 613 (1920).
[88] E. Ising, Z. Phys. **31**, 253 (1925).
[89] L. Onsager, Phys. Rev. **65**, 117 (1944).
[90] D. A. Lavis, *Equilibrium Statistical Mechanics of Lattice Models* (Springer, London, 2015).
[91] K. G. Wilson, Rev. Mod. Phys. **47**, 773 (1975).
[92] http://cluster_infap.unsl.edu.ar/wordpress/.